Electronic structure of PdSb

H. W. Myron and F. M. Mueller
Physics Laboratory and Research Institute for Materials, University of Nijmegen, Toernooiveld, Nijmegen, The Netherlands
(Received 4 November 1977)

The electronic band structure of PdSb has been calculated, as well as the density of states, joint density of states, optical transitions, and Fermi surface. In general there is good agreement with experimental results (when they exist). Comparison is also made to experimental results of other transition-metal compounds which crystallize in the NiAs or D^4_{6h} structure.

I. INTRODUCTION

The group of compounds which crystallize in the hexagonal NiAs or D^4_{6h} crystal structure continues to interest both theorists and experimentalists. Primarily this interest has centered on a number of anomalies in either the magnetic,[1] phononic,[2] or crystallographic[3] structures of several members of this group. In this paper we focus on PdSb—a material which as far as we know does not have such anomalies. The phase diagram of Pd_xSb_{1-x} near $x = 0.5$ shows a single-phase region and congruent melting.[4] Thus Pd and Sb form a highly stoichiometric compound in this region, and with care[5] single crystals may be grown with high resistivity ratios—of order 400. This is a sufficiently high stoichiometry that the accurate de Haas–van Alphen (dHvA) technique can be applied to measure the Fermi surface,[5] and in addition the optical properties,[6] and electron-spectroscopy-for-chemical-analysis (ESCA) spectra[7] were also available.

With such a wealth of experimental data, we envisioned that PdSb could be utilized as a "bench mark" material for the entire class of NiAs compounds and that a calculation of its electronic structure would be readily applicable to other systems. Previous calculations include those of Tyler and Fry,[8] Mattheiss,[9] and Kasowski[10] on NiS; England, Liu, and Myron on VS[11]; and a molecular-theory orbital band model of Goodenough *et al.*[12] It was our aim to utilize the several pieces of experimental data of PdSb to provide a best "adjusted" band structure of higher accuracy in that sense than previous calculations in other materials. In fact, as discussed below, a minimum adjustment was sufficient.

The plan of this paper is as follows: in Sec. II we give the formal aspects of our calculations; in Sec. III we give the band structure and the derived properties of the density of states, the joint density of states, the optical transitions, and the Fermi surface; in Sec. IV our conclusions are given.

II. CRYSTAL STRUCTURE, POTENTIAL, AND APW METHOD

As stated above, PdSb crystallizes in the hexagonal NiAs structure, space group D^4_{6h}. The lattice consists of hexagonal layers of Pd atoms separated by hexagonal layers of Sb atoms. The NiAs structure is given in Fig. 1(a) and the corresponding Brillouin zone (BZ) in Fig. 1(b). An examination of the crystal structure in Fig. 1(a) suggests that PdSb has a lattice which will be intermediate between that of a closed-packed elemental structure (hcp—such as Ti metal) and an open, loose structure (such as MoS_2). The full crystal potential was calculated by the Mattheiss method[13] from overlapping Hartree-Fock-Slater atomic-charge densities of Herman and Skillman[14] using Slater's local approximation[15] ($\alpha = 1$) to treat exchange. The atomic configurations are given in Table I.

With the two types of four atoms in the unit cell, some freedom exists in the choice of the various muffin-tin (MT) radii. Computational simplicity within the augmented-plane-wave[16] (APW) method dictates that these radii should be as large as possible, i.e., the Pd radius and the Sb radius touch. We imposed the additional criterion that the choice of radii should minimize the sum of the square of the discontinuities between the value of the spherically symmetric potentials *inside* the two types of MT radii and the value of the MT floor in the interstitial region. Although we have not made a detailed study of the point, we believe that this criterion provides a simple form of smoothest MT potential. The best choices for the radii are given in Table I. Direct examination of the full crystal

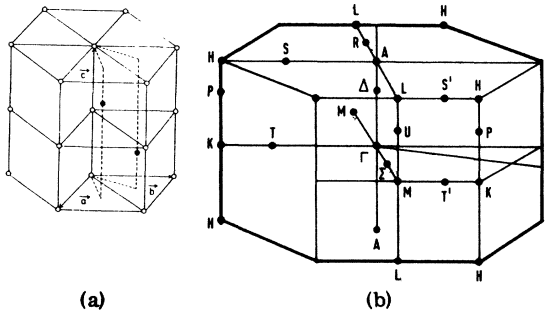

FIG. 1. (a) Nickel-arsenide or D^4_{6h} crystal structure. (b) The Brillouin zone of the D^4_{6h} structure.

TABLE I. Potential parameters used for PdSb.

Atomic configuration	Pd $(4d^9 5s^1)$ Sb $(5s^2 5p^3)$
Lattice constant[a]	$a = 4.076$ Å $c = 5.592$ Å
Muffin-tin radii	$R(\text{Pd}) = 2.254$ a.u.
	$R(\text{Sb}) = 2.895$ a.u.
Positions of atoms in unit cell	Pd: $(0, 0, 0)$
	$(0, 0, c/2)$
	Sb: $[(a/2\sqrt{3}), a/2, c/4]$
	$(a/\sqrt{3}, 0, 3c/4)$
Fraction of volume outside muffin-tin spheres	0.448
Zero of energy relative to vacuum	−1.036 Ry

[a] From Ref. 18.

potential and MT approximate with radii of Table I, showed modest differences in the inner region (of order 25 mRy) but larger differences in the interstitial region (of order 150 mRy), a result not too surprising in view of the "semi-loose" NiAs structure. We have therefore ignored the "inside" corrections, but have explicitly incorporated the "outside" corrections.

Since the outside corrections were large we have utilized the APW method for the band structure in which such outside corrections take a particularly simple form[17]; as a Fourier transform of the interstitial potential

$$V_{\text{out}}(\vec{r}) = \sum_b V_b e^{i\vec{b}\cdot\vec{r}}. \tag{1}$$

These effects are now called "warping." We have found the expansion coefficients V_b by direct numerical expansion, i.e., summing over 40 800 points in the interstitial region. The relevant parameters used in the band calculation are listed in Table I.

We developed a nonsymmetrized version of the APW method for the NiAs structure. Since the number of plane waves needed in order that the eigenvalues be converged to a few mRy is quite large for this crystal structure, care was taken to increase the speed of the computer programs and convergence rate of the eigenvalues. Some points are worth mentioning.

A variable basis for each point in the $\frac{1}{24}$th BZ is ordered in reciprocal space according to length. We find that the eigenvalues are converged to 3 mRy for general points in the BZ when approximately 220 ordered plane waves are used. The same degree of convergence is obtained for a fixed basis set of somewhat over 300 plane waves. In passing, it is worth noting that the convergence rates of different states s, p, and d are quite sensitive to the size of the basis set following the empirical rules of Mattheiss *et al.*[19] quite closely.

The APW basis set is of course energy dependent, it is therefore necessary to set up the matrix at various energies for a given $\vec{k}$ point in the BZ and search for the roots (when the determinant of the secular equation goes through a zero). This is time consuming and tedious. Hence several techniques were investigated to speed up the root searching procedure.

We have investigated a search procedure similar to that employed in the Korringer-Kohn-Rostoker (KKR) method.[20] The eigentrajectories are calculated on an energy interval and the roots of the secular matrix are predicted using a regula falsi procedure. This scheme yields all eigenvalues, including degenerate roots, in an energy interval of 0.1 Ry within two or three iterations. However, this scheme is quite time consuming[21] since the eigenvalues for a matrix of rank N must be calculated at each iterated energy.

In order to reduce the size of the matrix first-order Löwdin perturbation[22] was applied. We find that the speed of the program was greatly increased when incorporated with the eigentrajectory predictor, but the energy bands were shifted nonuniformly up to 30 mRy. This procedure is also inapplicable in the energy region of the logarithmic derivative asymptotes. At this point we calculated the secular matrix for a given $\vec{k}$ point on an energy grid, put the matrix in tridiagonal form and interpolated on the number of negative diagonal elements and the secular determinant. Even though this leads to more evaluations of the secular matrix, it is accurate and faster than calculating the eigenvalue trajectories.

III. RESULTS

A. Energy bands

Using the APW method and the root-searching procedures of Sec. II, the energy bands of PdSb were calculated on a uniform mesh of 45 points in the irreducible wedge ($\frac{1}{24}$th) of the BZ. This mesh in reciprocal space includes three layers; (i) the basal plane $k_z = 0$; (ii) the face $k_z = \pi/c$; and (iii) halfway between $k_z = \pi/2c$; with 15 uniformly distributed points per layer. (Because the unit cell is "tall" along the c axis, the BZ is correspondingly "short.") We have found this mesh to be sufficiently dense to interpolate the energy-band structure to a high accuracy as described below.

The energy bands of PdSb are shown in Fig. 2. The lowest energy regions extending from −0.360 to −0.115 Ry are derived from Sb s states. Above 0.065 Ry at Γ are Pd-derived d bands and Sb-derived p bands. A clear distinction cannot be made between the p and d bands. Covalent bonding and

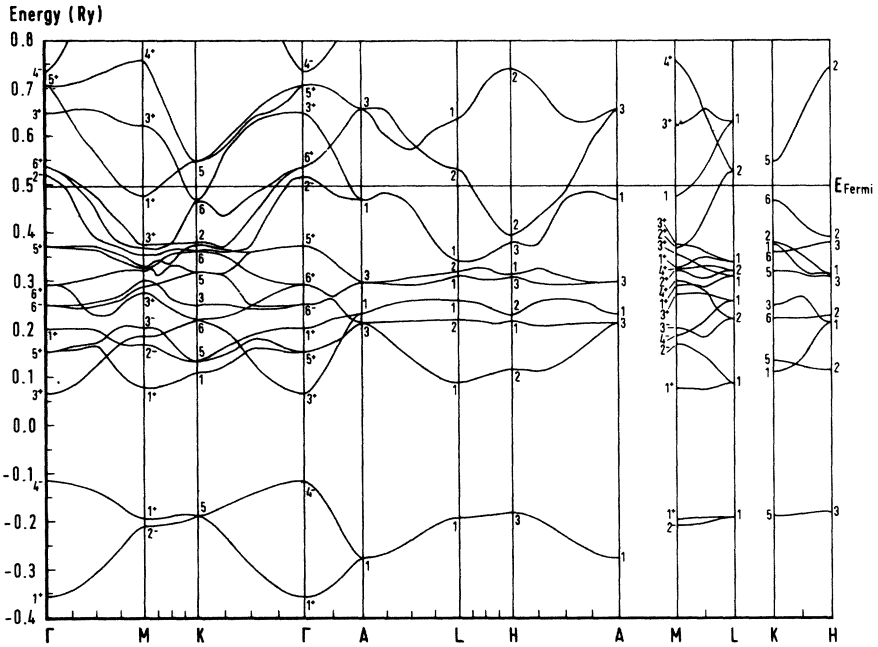

FIG. 2. Electronic energy-band structure of PdSb. The zero of energy has been shifted by −1.036 Ry.

mixing is strong in this material, since the Pd 4*d* atomic state lies just above the Sb 5*p* state. This general interpretation for the electronic structure of transition-metal antimonides has been suggested by Allen and Stutius based on their experimental data.[23]

TABLE II. Energy levels for PdSb at selected high-symmetry points with and without warping.

Γ	Muffin-tin	Muffin-tin corrected	*K*	Muffin-tin	Muffin-tin corrected
1^+	−0.350	−0.356	5	−0.180	−0.190
4^-	−0.110	−0.116	1	0.141	0.107
3^+	0.081	0.063	5	0.131	0.131
5^+	0.172	0.150	6	0.237	0.219
1^+	0.228	0.198	3	0.269	0.248
6^-	0.267	0.251	5	0.334	0.318
6^+	0.309	0.291	6	0.371	0.360
5^+	0.382	0.371	1	0.392	0.373
2^-	0.521	0.515	2	0.402	0.379
6^+	0.557	0.537	6	0.475	0.465
3^+	0.659	0.645	5	0.530	0.546
5^+	0.702	0.706			
A			*H*		
1	−0.270	−0.277	3	−0.172	−0.184
3	0.231	0.211	2	0.102	0.112
1	0.256	0.230	1	0.243	0.212
3	0.312	0.296	2	0.247	0.227
1	0.480	0.468	3	0.316	0.303
3	0.661	0.655	1	0.328	0.305
			3	0.392	0.379
			2	0.401	0.391
			2	0.736	0.742

The effect of including a nonspherical interstitial potential to the energy bands can be quite substantial for individual states. We find that states at high symmetry points change by as much as 0.034 Ry, but the ordering of the bands remains generally insensitive. The notable exception is the interchange of two states K_1 and K_5. The K_5 state at 0.131 Ry remains unchanged while the K_1 state lowers by 0.034 Ry and is below the K_5 state with the addition of MT corrections. A comparison of four high symmetry points Γ, *K*, *A*, and *H* for the two crystal potentials is shown in Table II.

B. Density of states

In order to calculate the density of states, we have interpolated each of the bands on the 45-point mesh onto a Fourier series as

$$E_n(\vec{k}) = \sum_{\vec{R}} C_{\vec{R}}^n e^{i\vec{k}\cdot\vec{R}}, \tag{2}$$

where as usual the set $C_{\vec{R}}^n$ was made equivalent over a star of equivalent $\vec{R}$'s. In order that the Fourier fit "average" the band structure *n* we have limited the expansion set to 27 stars.

The electronic structure was fit to the Fourier series by means of the least-squares procedure MINFIT.[24] The root-mean-square error for the 22 bands fit was not greater than 12 mRy, while the error for the bands below E_F was less than 6 mRy (the higher bands are wider). The density of states

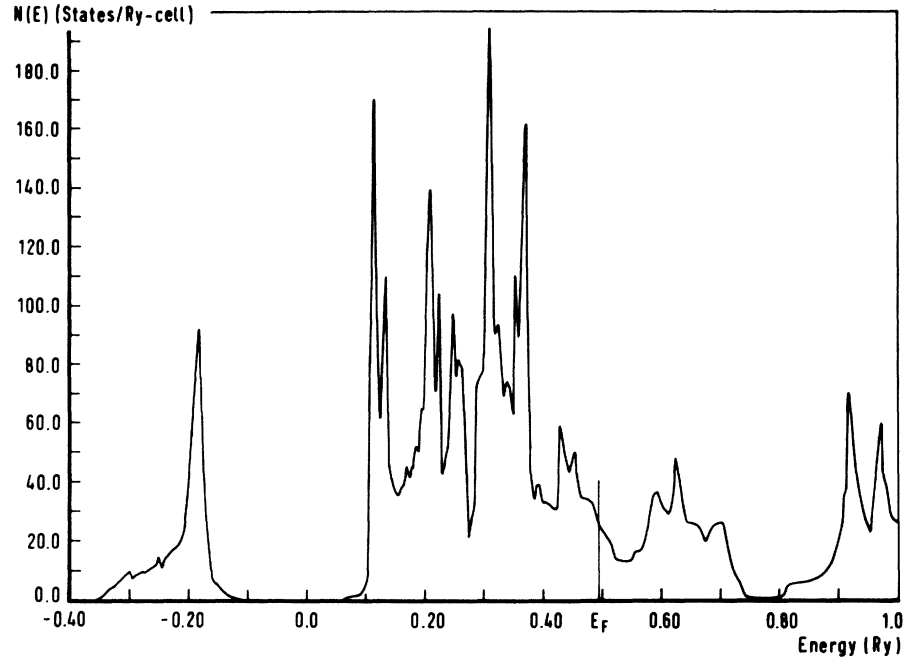

FIG. 3. Electronic density of states of PdSb.

is calculated using the linear tetrahedron method[25]; the number to tetrahedron needed to perform the Brillouin-zone integration is chosen such that no structure changes by more than 1%. This corresponds to choosing 5880 tetrahedrons in the $\frac{1}{24}$th BZ. $N(E)$ was calculated on an energy grid of 2 mRy in order to determine the density of states $n(E)$, and the Fermi energy accurately. Once E_F is determined, then the joint density of states (JDOS) is calculated along the same line as $N(E)$.

The density of states of PdSb shown in Fig. 3 can be broadly separated into two regions. The Sb s-band region from −0.350 to −0.125 Ry is clearly distinct and does not overlap with the higher Pd $4d$ and Sb $5p$ states. This result of a nonoverlapping nonmetal s band is also borne out by calculations of England *et al.*[11] for hypothetical vanadium sulfide in the NiAs structure. The separation of the sulfur s band in VS from the p-d manifold is of the order of 0.4 Ry and reflects the diminished overlap of the radial charge densities between the metal and nonmetal constituents in VS than PdSb.

Broadly speaking, the density of states above 0.065 Ry and below 0.450 Ry is composed of highly mixed Pd $4d$ and Sb $5p$ derived states. There is no clear distinction between the nonmetal-derived p bands from the metal-derived d bands as found in many transition-metal dichalcogenides,[26] but rather a high degree of mixed p and d states as found for $PdTe_2$.[27]

The Fermi energy of PdSb falls at 0.495 Ry above the peak structure of the density of states. The calculated density of states at the Fermi energy is 25 states/(Ry cell). This leads to a value of γ, the electronic contribution to the specific heat, of 1.16 mJ/mole°K². Low-temperature specific-heat measurements have not been reported to date.

General features of the density of states, can be compared to recent ESCA experiments of Van Attekum and Trooster.[7] The experimental findings indicate an s bandwidth of 3.0 eV, s to p-d band gap of 2.9 eV and a p-d bandwidth of 6.1 eV, these results agree quite well to our corresponding features of 3.13, 2.48, and 5.84 eV (see Table III). However, the central peak determined from the ESCA experiment lies approximately 1.0 eV below our calculated results.

Additionally, ESCA experiments[28] on MnSb tend to confirm the above findings. If we rigidly remove three electrons from the density of states of PdSb, corresponding to a new Fermi energy of 0.417 Ry

TABLE III. Calculated and experimental features of PdSb ESCA experiments.

	Calculated (eV)	Experimental (eV)
Width of s band	3.13	3.0
s to pd band gap	2.48	2.90
Width of pd band	5.84	6.10

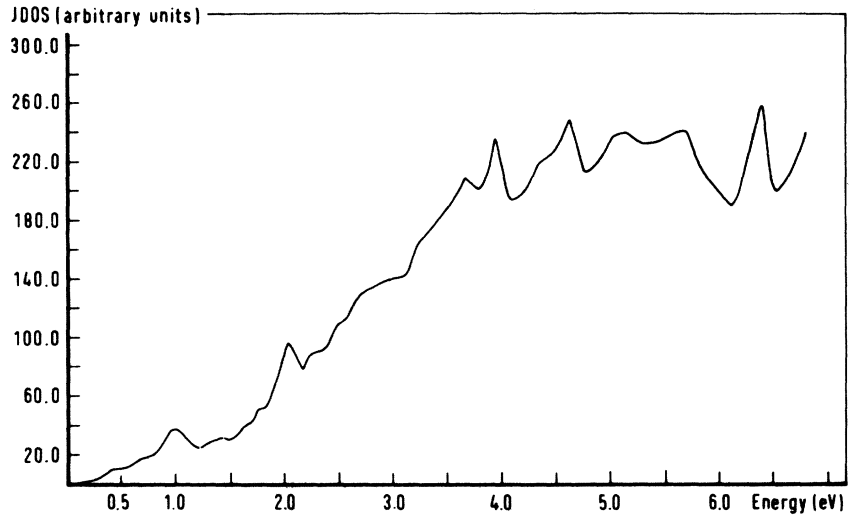

FIG. 4. Joint density of states of PdSb.

for "MnSb," then the calculated *pd* bandwidth becomes 4.31 eV which is quite close to the experiment value of 4.1 eV. Furthermore, the *s* to *pd* gap and the width of the *s* band remains the same as that of PdSb.

C. Joint density of states

Recent optical ellipsometry experiments on single crystal PdSb by Castelijns[6] indicate peak structure in the joint density of states at 1.5 and 2.0 eV and a shoulder at 3.7 eV. The JDOS increases rather linearly with energy above 4.0 eV. In order to make connection with the optical experiment we have calculated the JDOS of this material assuming constant dipole-matrix elements. We find similar peak structure at 1.0 and 2.1 eV. At higher photon energies considerably more structure is found: (i) maxima at 3.95, 4.63, and 6.42 eV; (ii) shoulders at 3.13, 3.68, 5.00, and 5.71 eV; and (iii) minima at 4.08, 4.79, 6.13, and 6.55 eV. The computed JDOS is shown in Fig. 4.

The sharp drop in the JDOS above 5.71 eV corresponds to excitations below the bottom of the *pd* band. This agrees well with the width of the *pd* band as measured by ESCA.[7] Unfortunately, this drop is not seen in the ellipsometry results, since the optical source was not considered monochromatic above 5 eV.

As is customary, identifications of peaks in the JDOS can be made from the band structure as to where in the Brillouin zone and which initial and final states contribute substantially. These identifications are listed in Table IV.

Optical reflectivity measurements have been recently published on other transition-metal antimonides by Allen and Mikkelsen.[29] We will focus our

TABLE IV. Decomposition of optical transitions for PdSb.

Energy (eV)	Direction	Location	Initial	Final
1.0	ΓM	$\frac{1}{2}$–$\frac{3}{4}$ ΓM	15	16
		$K_6 \rightarrow K_5$	15,16	17,18
			15	16
2.1	ΓK	0.42–0.76 ΓK	15	16,17,18
	AL	0.62–0.75 AL	13,14	15,16
3.95	ΓM	0.25 ΓM–M	12,13	18
	AL	0.35–0.75 AL	10,11	16,17
			12,13	18,19
	ML	0.5 ML–L	14,15	19
4.63	ΓM	Γ–0.43 ΓM	11,12	18
	ΓK	Γ–0.43 ΓK	10	16,17,18
	ΓA	Γ–0.5 ΓA	6	14,15

attention on NiSb since it has the same electronic configuration as PdSb. The infered *pd* bandwidth of NiSb determined by reflectivity measurments and Kramers-Kronig analysis is approximately 5 eV. This is somewhat lower than the *pd* bandwidth in PdSb from ESCA (6.1 eV) or from our results, but clearly reflects the narrowing of the *d* band of NiSb relative to PdSb. This difference in the *pd* bandwidth of almost 1.1 eV for these two isoelectronic compounds can be nearly accounted for by assuming the metal-derived *d* bands narrow the same in the transition-metal antimonide as the transition metal.

D. Fermi surface and de Haas-van Alphen effect

Considerable experimental effort has been expended in measuring the dHvA frequencies of compounds with the NiAs crystal structure. We will limit our discussion to AuSn,[30,31] PtSn,[32,33] and PdSb,[5] since these materials are isoelectronic. The models[30] used to understand the Fermi surface (FS) are derived from a single orthogonalized plane wave (1-OPW) and the Harrison[34] construction. This model has been successful in explaining the FS when modified slightly by the experimental realities.

However, to date there has been no *ab initio* attempt to construct a FS for any of these three materials. Using the electronic structure of PdSb a FS was constructed which yielded similar topological forms deduced from dHvA experiments and the 1-OPW model, but whose frequencies were in error by 15%–20%. In order to correct this difficulty we shifted the *ab initio* E_F upward by 0.020 Ry. This corresponds to an error of 0.3 electrons in the number density of states or 1% of the total number of electrons below E_F. The adjusted FS cross sections are shown in Fig. 5. The designations 3, 4, 5, and 6 correspond to the fourteenth, fifteenth, sixteenth, and seventeenth band (from the bottom of the band structure) crossing E_F.

Cross-section 3 is designated as a hole orbit centered around the ΓA line—the three-dimensional picture corresponds closely to zones 3 and 4 of the 1-OPW model[31] [see Fig. 6(a)]. We call this orbit the "dog's bone."

The dog's bone orbit can support at most four frequencies in the ⟨0001⟩, ⟨10$\bar{1}$0⟩, and ⟨11$\bar{2}$0⟩ field directions. For the ⟨0001⟩ field we calculate two orbits, the first is the Γ-centered orbit in the ΓMK plane designated as μ,[31,33] and the second is a noncentral orbit situated along the ΓA line approximately 80% of the way from Γ to A. This orbit has been designated as σ.[33] The frequencies of the μ and σ orbits in the ⟨0001⟩ direction are calculated as 4.9 and 35.7 MG, respectively. The two other orbits in the ⟨10$\bar{1}$0⟩ and ⟨11$\bar{2}$0⟩ originate from the ΓKHA and ΓMLA faces of the BZ, respectively, we designate this orbit as ϕ whose frequencies are 30.0 and 38.4 MG, respectively.

Cross-section 4 also supports four orbits Fig. 6(b), the δ and λ in the ⟨0001⟩ field direction, the δ in the ⟨10$\bar{1}$0⟩ and ⟨11$\bar{2}$0⟩, and the (unmeasured) ψ in the ⟨11$\bar{2}$0⟩ direction. This hole surface is best described as central pillar perpendicular to the basal plane with arms directed along the AL direction. The δ orbit is formed by the hole piece centered at Γ and has a frequency of 11.5 MG in ⟨0001⟩ field,

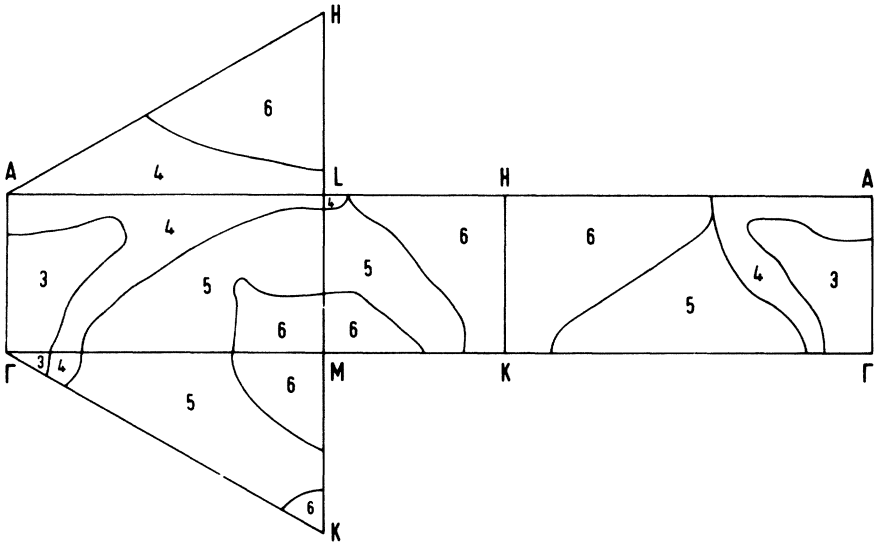

FIG. 5. Fermi surface of PdSb. As explained in the text, the band Fermi level was shifted upward by 20 mRy. This adjustment is consistent with the 1% accuracy of the density of states, Fig. 3.

while the λ frequency of 75.1 is formed on the ALH face surrounding H. The λ and γ orbits (from cross-section 6) are degenerate since spin-orbit coupling has not been included in these calculations. The δ hole orbits centered about the L point are quite small with frequencies of 1.3 and 1.1 MG in the $\langle 11\bar{2}0\rangle$ and $\langle 10\bar{1}0\rangle$ direction. The ψ orbit in $\langle 11\bar{2}0\rangle$ direction calculated at 98.6 MG is observed in PtSn but not in AuSn. A search for this piece is now in progress at the Nijmegen High Field Magnet facility.[35]

Cross-section 5 does not yield any closed orbits but rather open orbits in the $\langle 10\bar{1}0\rangle$ field direction. A galvanometric investigation of the FS of AuSn has also suggested open orbits along the $\langle 10\bar{1}0\rangle$ direction.[35]

The FS of cross-section 6 is a two-sheeted electron surface and is topologically equivalent to zone 6 of the modified 1-OPW model[31,33] [Fig. 6(c)]. These orbits have previously been described as "humbugs" situated around the HK line and "butterflies" surrounding M. The humbugs yield two oscillations in the $\langle 0001\rangle$ field direction, the α orbit forms the waist of the humbug surrounding the K point having a frequency of 4.0 MG and the second the γ orbit surrounding the H point has a frequency of 75.1 MG. There is possibly a third orbit designated as ζ, which has not been measured in PdSb, but would have a frequency of 21.1 MG in the $\langle 11\bar{2}0\rangle$ direction and would disappear quickly for field orientations away from this symmetry direction. This orbit has been observed in AuSn,[30,31] but not in PtSn.[32,33] The so-called butterfly orbits have the symmetry of the M point and yield frequencies β in $\langle 0001\rangle$ direction of 16.9 MG and ϵ orbits of 17.6 and 18.9 MG in the $\langle 10\bar{1}0\rangle$ and $\langle 11\bar{2}0\rangle$ directions.

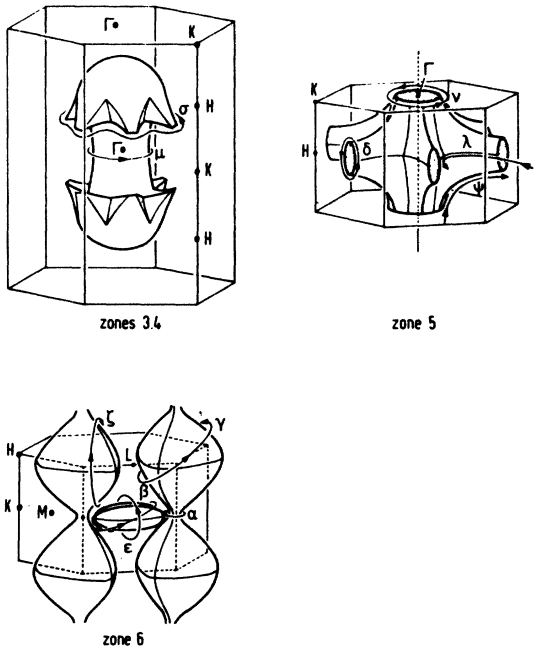

FIG. 6. Three-dimensional Fermi surface models (Ref. 33): (a) zones 3 and 4; (b) zone 5; and (c) zone 6.

TABLE V. Extremal cross-sectional frequencies for PdSb.

Field direction	Orbit	Frequency (MG) Theory	Experiment (Ref. 6)
$\langle 0001\rangle$	α	4.0	3.11
	μ	4.9	···
	ν	11.5	5.05
	β	16.9	18.3
	σ	35.7	···
	γ	75.1	72.0
	λ	75.1	77.0
$\langle 11\bar{2}0\rangle$	δ	1.3	2.27
	ϵ	18.9	15.8
	ζ	21.1	···
	ϕ	38.3	···
	ψ	98.6	···
$\langle 10\bar{1}0\rangle$	δ	1.1	1.95
	$A5$	···	4.98
	ϵ_1	17.6	15.7
	ϵ_2	20.3	19.0
	ϕ	30.0	37.7

A summary of all the calculated and experimental orbits is made in Table V.

Finally, two cyclotron masses have been calculated in the $\langle 0001\rangle$ field direction. In units of the free-electron mass, the λ and γ masses are 0.43, which should be compared to 0.49 and 0.52 in PtSn,[33] and 0.636 in AuSn,[31] for λ and γ, respectively. The calculated β mass in PdSb is 0.28, while the corresponding is measured as 0.37 and 0.34 in PtSn,[33] and AuSn,[31] respectively. A critical test of our adjusted FS with experimental cyclotron masses is desirable, but these are, however, presently not available.

IV. DISCUSSION AND CONCLUSION

We have calculated the electronic structure of PdSb using the APW method and have included the important corrections to the potential in the interstitial region. By adjusting the Fermi level by 20 mRy, the calculated Fermi surface is in excellent agreement with several observed orbits. In addition, we have predicted several other extremal orbits. By comparison to ESCA and optical properties, we conclude that our bands are in good agreement with experiments on PdSb. Several

other features are predicted. We anticipate, however, that our PdSb bands will be most useful to experimentalists in interpreting results in other NiAs structure materials.

ACKNOWLEDGMENTS

This work was performed as part of the research program of the Stichting voor Fundamenteel Onderzoek der Materie (FOM) with financial support from the Nederlandse Organisatie voor Zuiver Wetenschappelijk Onderzoek (ZWO). The authors would like to thank Dr. P. van Attekum, Dr. J. Trooster, Professor A. R. de Vroomen, and Dr. J. Castelijns for communicating their unpublished results and special thanks to Dr. M. Devillers for discussions on the de Haas–van Alphen section.

[1]J. T. Sparks and T. Komoto, J. Appl. Phys. 34, 1191 (1963); 39, 715 (1968); Rev. Mod. Phys. 40, 752 (1968).
[2]S. H. Liu, Phys. Rev. B 10, 3619 (1974).
[3]H. F. Franzen and T. J. Burger, J. Chem. Phys. 49, 2268 (1968); H. F. Franzen, C. Haas, and F. Jellinek, Phys. Rev. B 10, 1248 (1974).
[4]M. Hansen, *Constitution of Binary Alloys*, 2nd ed. (McGraw-Hill, New York, 1958), p. 1124.
[5]N. J. Coenen, C. A. J. Morsing, A. P. J. M. Reyers, and L. W. M. Schreuers, Solid State Commun. 16, 557 (1975); N. J. Coenen, thesis (Katholieke Universiteit van Nijmegen, 1976) (unpublished).
[6]J. H. P. Castelijns, thesis (Katholieke Universiteit van Nijmegen, 1977) (unpublished).
[7]P. M. Th.M. van Attekum and J. M. Trooster (private communication).
[8]J. M. Tyler and J. L. Fry, Phys. Rev. B 1, 4604 (1970).
[9]L. F. Mattheiss, Phys. Rev. B 10, 995 (1974).
[10]R. V. Kasowski, Phys. Rev. B 8, 1378 (1973); Solid State Commun. 14, 103 (1974).
[11]W. B. England, S. H. Liu, and H. W. Myron, J. Chem. Phys. 60, 3760 (1974).
[12]J. B. Goodenough and J. A. Kafalas, Phys. Rev. 157, 389 (1967); N. Menyuk, J. A. Kafalas, K. Dwight, and J. B. Goodenough, *ibid.* 177, 942 (1969).
[13]L. F. Mattleiss, Phys. Rev. 133, A1399 (1964).
[14]F. Herman and S. Skillman, *Atomic Structure Calculations* (Prentice-Hall, Englewood Cliffs, N. J., 1963).
[15]J. C. Slater, Phys. Rev. 81, 385 (1951).
[16]J. C. Slater, Phys. Rev. 51, 846 (1937).
[17]P. D. De Ciccio, Phys. Rev. 153, 931 (1967).
[18]J. N. Pratt, K. M. Myles, J. B. Darby, and M. H. Mueller, J. Less-Common Metals 14, 427 (1968).
[19]L. F. Mattheiss, J. H. Wood, and A. C. Switendick, in *Methods in Computational Physics*, edited by B. Adler, S. Fernbach, and M. Rotenberg (Academic, New York, 1968).
[20]J. C. Shaw, J. B. Ketterson, and L. R. Windmiller, Phys. Rev. B 5, 3894 (1972).
[21]B. T. Smith, J. M. Boyle, B. S. Garbow, Y. Ikebe, V. C. Klema, and C. B. Muler, *Matrix Eigensystem Routines—Eispack Guide* (Springer-Verlag, Berlin, 1974).
[22]P. O. Löwdin, J. Chem. Phys. 19, 1396 (1951).
[23]J. W. Allen and W. Stutius, Solid State Commun. 20, 561 (1976).
[24]B. S. Garbow and J. J. Dongarra, Path Chart and Documentation for Eispack Package of Matrix Eigensystem Routines, Tech. Mem. No. 250 (Argonne National Laboratory, updated 1975) (unpublished).
[25]G. Lehmann, P. Rennert, M. Taut, and H. Wonn, Phys. Status Solidi 37, K27 (1970); G. Lehmann and M. Taut, *ibid.* 54, 469 (1972); O. Jepsen and O. K. Andersen, Solid State Commun. 9, 1763 (1971).
[26]L. F. Mattheiss, Phys. Rev. B 8, 3719 (1973); H. W. Myron and A. J. Freeman, *ibid.* 9, 481 (1974).
[27]H. W. Myron, Solid State Commun. 15, 395 (1974).
[28]R. A. de Groot, thesis (Rijksuniversiteit Groningen, 1976) (unpublished); T. Chen and K. S. Liang, in Fifth International Conference on Solid Compounds of Transition Elements, Uppsala, 1976, Extended Abstracts, p. 5 (unpublished).
[29]J. W. Allen and J. C. Mikkelsen, Phys. Rev. B 15, 2952 (1977).
[30]G. J. Edwards, W. B. Pearson, Y. Saito, and M. Springford, in Tenth International Conference on Low Temperature Physics, 1966) (unpublished).
[31]G. J. Edwards, M. Springford, and Y. Saito, J. Phys. Chem. Solids 30, 2527 (1970).
[32]J.-P. Jan, W. B. Pearson, and M. Springford, Can. J. Phys. 42, 2357 (1964).
[33]W. N. Cathey, P. T. Coleridge, and J.-P. Jan, Can. J. Phys. 48, 1151 (1970).
[34]W. A. Harrison, Phys. Rev. 116, 555 (1969).
[35]M. A. C. Devillers and H. W. Myron (unpublished).
[36]D. J. Sellmyer and P. A. Schroeder, Phys. Lett. 16, 100 (1965).